IOPscience iopscience.iop.org

Home Search Collections Journals About Contact us My IOPscience

Ising t–J model close to half filling: a Monte Carlo study

This article has been downloaded from IOPscience. Please scroll down to see the full text article.

2009 J. Phys.: Condens. Matter 21 045703

(http://iopscience.iop.org/0953-8984/21/4/045703)

View the table of contents for this issue, or go to the journal homepage for more

Download details:
IP Address: 129.252.86.83
The article was downloaded on 29/05/2010 at 17:30

Please note that terms and conditions apply.

J. Phys.: Condens. Matter **21** (2009) 045703 (13pp) doi:10.1088/0953-8984/21/4/045703

Ising t–J model close to half filling: a Monte Carlo study

M M Maśka[1], M Mierzejewski[1], A Ferraz[2] and E A Kochetov[3]

[1] Department of Theoretical Physics, Institute of Physics, University of Silesia, 40-007 Katowice, Poland
[2] International Center of Condensed Matter Physics, Universidade de Brasilia, Caixa Postal 04667, 70910-900 Brasilia, DF, Brazil
[3] Laboratory of Theoretical Physics, Joint Institute for Nuclear Research, 141980 Dubna, Russia

Received 21 October 2008, in final form 4 December 2008
Published 8 January 2009
Online at stacks.iop.org/JPhysCM/21/045703

Abstract
Within the recently proposed doped-carrier representation of the projected lattice electron operators we derive a full Ising version of the t–J model. This model possesses the global discrete Z_2 symmetry as a maximal spin symmetry of the Hamiltonian at any values of the coupling constants, t and J. In contrast, in the spin anisotropic limit of the t–J model, usually referred to as the t–J_z model, the global $SU(2)$ invariance is fully restored at $J_z = 0$, so that only the spin–spin interaction has in this model the true Ising form. We discuss a relationship between these two models and the standard isotropic t–J model. We show that the low-energy quasiparticles in all three models share qualitatively similar properties at low doping and small values of J/t. The main advantage of the proposed Ising t–J model over the t–J_z one is that the former allows for the unbiased Monte Carlo calculations on large clusters of up to 10^3 sites. Within this model we discuss in detail the destruction of the antiferromagnetic (AF) order by doping as well as the interplay between the AF order and hole mobility. We also discuss the effect of the exchange interaction and that of the next-nearest-neighbour hoppings on the destruction of the AF order at finite doping. We show that the short-range AF order is observed in a wide range of temperatures and dopings, much beyond the boundaries of the AF phase. We explicitly demonstrate that the local no-double-occupancy constraint plays the dominant role in destroying the magnetic order at finite doping. Finally, a role of inhomogeneities is discussed.

(Some figures in this article are in colour only in the electronic version)

1. Introduction

Since the discovery of the high-temperature superconductors (HTSCs), many theoretical investigations have been focused on the study of the doping evolution from the antiferromagnetically ordered Mott insulator to the BCS-type superconductor. It is commonly assumed that this evolution is the key ingredient for the understanding of the physics behind high-temperature superconductivity and it can adequately be addressed in terms of the two-dimensional (2D) t–J lattice model. This model is believed to capture the essential low-energy physics of doped Mott insulators driven by strong electron correlations. Although it is generally accepted that strong electron correlations play an important role close to half filling, it remains unclear to what extent HTSCs can be described entirely in terms of this minimal electronic model.

One of the reasons for this lack of clarity is that, despite its simplicity, the exact properties of the t–J model, apart from a few limiting cases, are still unknown. The vast majority of the results away from half filling have been obtained for one or two holes introduced into the AF background. This problem has been thoroughly analysed with the help of various analytical and numerical approaches [1–11]. Results for larger dopings are less comprehensive. Here, one of the important problems concerns the robustness of the AF order against doping. Most of the theoretical approaches predict that the long-range AF order persists up to much larger dopings than observed in cuprates [12, 13]. It has recently been suggested that including in consideration the nearest-neighbour hopping may help in resolving this discrepancy [14]. However, a reliable and well controlled analytical treatment of the isotropic t–J model poses a severe technical problem: it is very hard to analytically

 © 2009 IOP Publishing Ltd Printed in the UK

deal with the local no-double-occupancy (NDO) constraint. On the other hand, because of this constraint, numerical treatment is available only on rather small lattice clusters, which immediately raises the problem of the finite-size effects and, consequently, of the thermodynamical stability of the results obtained.

An interesting question then arises: is there available a modification of the isotropic t–J model that allows for unbiased numerical treatment and at the same time captures the essential properties of the original t–J model, at least for a certain parameter range? Some of the computational difficulties related to the t–J model may be overcome by means of investigations of its anisotropic limit, i.e. the t–J_z model. Numerical work has suggested that the t–J and t–J_z models have many similar properties [15]. In particular, the stripes, pairing, and Nagaoka states found in the t–J_z model are very similar to those of the isotropic t–J model [16–20]. In general, despite some significant differences between both the models [20, 21], at the low-energy scale of order J ($\ll t$) it is reasonable to consider the background spin configuration to be frozen with respect to the hole dynamics timescale. In this case the properties of the low-energy quasiparticle excitations in the t–J model are at least qualitatively similar to those in the anisotropic t–J_z model. Although this model is more amenable to numerical calculations, again only rather small lattice clusters are allowed.

One may hope that the full Ising version of the t–J model in which the t-term possesses the global discrete Z_2 spin symmetry rather than the $SU(2)$ one results in a more tractable though still nontrivial model. However, it is not clear how such a model can be derived directly in terms of the Gutzwiller-projected lattice electron operators, since those operators transform themselves in a fundamental representation of $SU(2)$. In this paper we use the recently proposed doped-particle representation of the projected electron operators to derive the full Ising version of the t–J model. We believe that the results of our study capture some essential low-energy properties of the isotropic t–J model since the strongly correlated nature of the problem is preserved.

The doped-particle representation of the t–J model is especially suited for investigations of the underdoped regime [22–24]. Some crucial points of this approach are recalled at the beginning of the following section. Although this is a slave-particle formulation, it differs from other similar approaches in that the NDO constraint is identically fulfilled at half filling. Since the holes are the only charge degrees of freedom present in the system, the number of charge carriers is very small close to half filling. Therefore, this approach is particularly useful for the description of the underdoped regime, whereas its applicability to the description of strongly overdoped cuprates is much more involved.

Until now, the doped-particle representation has been analysed only within mean-field approximations [22, 23]. Our aim is to go beyond this approximation in such a way that the slave-particle constraint is exactly taken into account. We demonstrate that this can be achieved for very large clusters of the order of 10^3 lattice sites, provided the $SU(2)$ symmetry is broken down to Z_2 not only in the spin–spin interaction term but also in the hopping term. Since the effectiveness of the resulting calculations is independent of the translational invariance, this approach also allows one to investigate the role of inhomogeneities which are expected to play an important role in the cuprate compounds [25].

The paper is organized as follows. Section 2 describes in detail the derivation of the theoretical model. Section 3 comprises the results of the numerical calculations. Section 4 lists our conclusions.

2. Model and approach

2.1. Doped-carrier formulation of the t–J model

We start with the t–J Hamiltonian on a square lattice [26]

$$H_{tJ} = -\sum_{ij\sigma} t_{ij}\tilde{c}^{\dagger}_{i\sigma}\tilde{c}_{j\sigma} + J\sum_{\langle ij\rangle}(\boldsymbol{Q}_i\boldsymbol{Q}_j - \tfrac{1}{4}\tilde{n}_i\tilde{n}_j), \qquad (1)$$

where $\tilde{c}_{i\sigma} = Pc_{i\sigma}P = c_{i\sigma}(1-n_{i,-\sigma})$ is the projected electron operator (to exclude the onsite double occupancy), $\boldsymbol{Q}_i = \sum_{\sigma,\sigma'}\tilde{c}^{\dagger}_{i\sigma}\boldsymbol{\tau}_{\sigma\sigma'}\tilde{c}_{i\sigma'}$, $\tau^2 = 3/4$, is the electron spin operator and $\tilde{n}_i = Pn_iP = n_{i\uparrow} + n_{i\downarrow} - 2n_{i\uparrow}n_{i\downarrow}$. Hamiltonian (1) contains a kinetic term with the hopping integrals t_{ij} and a potential J describing the strength of the nearest neighbour spin exchange interaction. At every lattice site the Gutzwiller projection operator $P = \prod_i(1 - n_{i\sigma}n_{i-\sigma})$ projects out the doubly occupied states $|\uparrow\downarrow\rangle$, thereby reducing the quantum Hilbert space to a product of three-dimensional spaces spanned by the states $|0\rangle_i$, $|\uparrow\rangle_i$ and $|\downarrow\rangle_i$. Physically, this modification of the original Hilbert space results in strong electron correlation effects. The crucial local no-double-occupancy constraint is rigorously incorporated into equation (1). However, this is achieved at the expense of introducing the constrained electron operators, $\tilde{c}^{\dagger}_{i\sigma}$, that obey much more complicated commutation relations than the conventional 'unconstrained' fermion operators. It should be stressed that it is precisely close to half filling where the Gutzwiller projection is of crucial importance: the projected electron operator $\tilde{c}^{\dagger}_{i\sigma}$ in this regime significantly differs from the bare electron operator $c^{\dagger}_{i\sigma}$ (right at half filling $\tilde{c}^{\dagger}_{i\sigma} = 0$).

A natural question then arises: is it possible to rewrite the t–J Hamiltonian in terms of the conventional fermion and spin operators in such a way that the NDO constraint for the lattice electrons transforms itself into one that can be treated, close to half filling, in a controlled way? Recently, it has been shown that the t–J Hamiltonian can indeed be represented in this form [23, 22, 24].

For the reader's convenience we sketch below the main points of this scheme. The basic idea behind this approach is to assign fermion operators to doped carriers (holes, for example) rather than to the lattice electrons. The t–J Hamiltonian is expressed then in terms of the lattice spin operators, $\boldsymbol{S}_i$, and doped-carrier operators represented by spin-1/2 charged fermions, $d_{i\sigma}$.

To accommodate these new operators one obviously needs to enlarge the original onsite Hilbert space of quantum states. This enlarged space is characterized by the state vectors $|\sigma a\rangle$ with $\sigma = \Uparrow, \Downarrow$ labelling the spin projection of the lattice spins

and $a = 0, \uparrow, \downarrow$ labelling the dopon states (double occupancy is not allowed). In this way the enlarged Hilbert space becomes

$$\mathcal{H}_i^{\mathrm{enl}} = \{|\Uparrow 0\rangle_i, |\Downarrow 0\rangle_i, |\Uparrow\downarrow\rangle_i, |\Downarrow\uparrow\rangle_i, |\Uparrow\uparrow\rangle_i, |\Downarrow\downarrow\rangle_i\}, \tag{2}$$

while in the original Hilbert space we can either have one electron with spin σ or a vacancy:

$$\mathcal{H} = \{|\uparrow\rangle_i, |\downarrow\rangle_i, |0\rangle_i\}. \tag{3}$$

The following mapping between the two spaces is then defined [22]:

$$|\uparrow\rangle_i \leftrightarrow |\Uparrow 0\rangle_i, \qquad |\downarrow\rangle_i \leftrightarrow |\Downarrow 0\rangle_i, \tag{4}$$

$$|0\rangle_i \leftrightarrow \frac{|\Uparrow\downarrow\rangle_i - |\Downarrow\uparrow\rangle_i}{\sqrt{2}}. \tag{5}$$

The remaining states in the enlarged Hilbert space, $(|\Uparrow\downarrow\rangle_i + |\Downarrow\uparrow\rangle_i)/\sqrt{2}$, $|\Uparrow\uparrow\rangle_i$, $|\Downarrow\downarrow\rangle_i$ are unphysical and should therefore be removed in actual calculations. In this mapping, a vacancy in the electronic system corresponds to a singlet pair of a lattice spin and a dopon, whereas the presence of an electron is related to the absence of a dopon.

The spin–dopon representation of the t–J Hamiltonian then reads [24]

$$H_{t-J} = \sum_{ij\sigma} 2t_{ij}\tilde{d}^{\dagger}_{i\sigma}\tilde{d}_{j\sigma} + J\sum_{\langle ij\rangle}[(\boldsymbol{S}_i + \boldsymbol{M}_i)(\boldsymbol{S}_j + \boldsymbol{M}_j) - \tfrac{1}{4}(1-\tilde{n}^d_i)(1-\tilde{n}^d_j)], \tag{6}$$

with $\tilde{d}_{i\sigma} = d_{i\sigma}(1 - d^{\dagger}_{i,-\sigma}d_{i,-\sigma})$ being a projected dopon operator and $\tilde{n}^d_i = \sum_\sigma \tilde{d}^{\dagger}_{i\sigma}\tilde{d}_{i\sigma}$.

The application of H_{t-J} in this form should be accompanied by the implementation of the constraint to eliminate the unphysical states,

$$\boldsymbol{S}_i\boldsymbol{M}_i + \tfrac{3}{4}\tilde{n}^d_i = 0, \tag{7}$$

where $\boldsymbol{M}_i = \sum_{\sigma,\sigma'}\tilde{d}^{\dagger}_{i\sigma}\boldsymbol{\tau}_{\sigma\sigma'}\tilde{d}_{i\sigma'}$ stands for the dopon spin operator so that $\boldsymbol{Q}_i = \boldsymbol{S}_i + \boldsymbol{M}_i$. Note the important factor of 2 in front of the first term in equation (6). It originates from the fact that the vacancies are represented in this theory by the spin–dopon singlets given by equation (5). The projected lattice electron operators can be explicitly expressed in terms of the projected dopon operators. For example,

$$\tilde{c}^{\dagger}_{i\uparrow} = \sqrt{2}\mathcal{P}^{\mathrm{ph}}_i\tilde{d}_{i\downarrow}\mathcal{P}^{\mathrm{ph}}_i = \tfrac{1}{\sqrt{2}}[(\tfrac{1}{2} + S^z_i)\tilde{d}_{i\downarrow} - S^+_i\tilde{d}_{i\uparrow}], \tag{8}$$

where $\mathcal{P}^{\mathrm{ph}}_i = 1 - (\boldsymbol{S}_i\boldsymbol{M}_i + \frac{3}{4}\tilde{n}^d_i)$ is the projection operator which eliminates the unphysical states from the ith site.

The above representation of the t–J Hamiltonian is particularly useful for the description of strongly underdoped cuprates. Close to half filling $n^d_i \ll 1$, so that one can safely drop the tilde sign from the projected dopon operators. This is due to the fact that in the low doping regime the probability for the realization of a doubly occupied dopon state is indeed very low. Despite this, the NDO constraint (7) must be imposed to eliminate the unphysical degrees of freedom that are present in this formalism at any finite doping. Note, however, that at half filling the left hand side of equation (7) vanishes, and thus, in contrast to the original NDO constraint for the lattice electrons, this equation turns into a trivial identity[4]. Additionally, in this regime one can neglect both the hole–hole interactions represented by the $\boldsymbol{M}_i\boldsymbol{M}_j$ term, and the $\tilde{n}^d_i\tilde{n}^d_j$ couplings. Note also that the insulating phase in this representation is directly associated with the absence of charged particles.

2.2. The t–J_z and the Ising t–J models

So far, the doped-particle representation of the t–J model has been analysed only within the mean-field approximations [23, 22, 24]. Our aim is to go beyond the mean-field analysis and to carry out calculations for large enough systems, to make sure that the finite-size effects are truly negligible. Let us start with the anisotropic limiting case of the t–J model with the spins polarized only along the z-component, namely, the t–J_z model. This model is of interest in itself since it captures some essential physics of strong electron correlations.

The t–J_z model can be considered as a limiting case of the t–J model (1) which has an Ising rather than a Heisenberg spin interaction:

$$H_{t-J_z} = -\sum_{ij\sigma} t_{ij}\tilde{c}^{\dagger}_{i\sigma}\tilde{c}_{j\sigma} + J_z\sum_{\langle ij\rangle}(Q^z_iQ^z_j - \tfrac{1}{4}\tilde{n}_i\tilde{n}_j), \tag{9}$$

Here $\tilde{c}_{i\sigma}$ represent the Gutzwiller-projected electron operators. The global continuous spin $SU(2)$ symmetry of the t–J model now reduces to the global discrete Z_2 symmetry of the t–J_z model. Although $Q^z_iQ^z_j$ interaction possesses discrete Z_2 symmetry, the original $SU(2)$ symmetry of all other terms of the Hamiltonian is preserved. Therefore, the symmetry of the t–J_z model depends on whether J_z is zero or finite. Namely, for $J_z = 0$ the $SU(2)$ symmetry is restored again. In contrast, in the full t–J model both the t- and J-terms possess the same $SU(2)$ symmetry.

It is therefore natural to seek a representation of the full Ising version of the t–J model in which the symmetry of the model does not depend on the values of the model parameters. Such a representation can straightforwardly be derived within the dopant–particle formulation of the t–J model. The physical consequences as well as computational advantages of such an approach will be discussed in the subsequent sections.

To proceed, we start right from the original t–J Hamiltonian described in terms of the lattice electrons given by equation (1), where we now put $Q^+_i = Q^-_i = 0$ at the operator level. We then have for the physical electron-projected operators

$$\begin{aligned}\tilde{c}_{i\uparrow} &= \mathcal{P}^{\mathrm{ph}}_i\tilde{d}^{\dagger}_{i\downarrow}\mathcal{P}^{\mathrm{ph}}_i = (\tfrac{1}{2} + S^z_i)\tilde{d}^{\dagger}_{i\downarrow},\\ \tilde{c}_{i\downarrow} &= \mathcal{P}^{\mathrm{ph}}_i\tilde{d}^{\dagger}_{i\uparrow}\mathcal{P}^{\mathrm{ph}}_i = (\tfrac{1}{2} - S^z_i)\tilde{d}^{\dagger}_{i\uparrow},\end{aligned} \tag{10}$$

where the projection operator now reads $\mathcal{P}^{\mathrm{ph}}_i = 1 - (2S^z_iM^z_i + \tilde{n}^d_i/2)$. It can easily be checked that

$$Q^+_i = (Q^-_i)^{\dagger} = \tilde{c}^{\dagger}_{i\uparrow}\tilde{c}_{i\downarrow} \equiv 0.$$

[4] The original local NDO constraint for the lattice electrons, $\sum_\sigma c^{\dagger}_{i\sigma}c_{i\sigma} \leqslant 1$, right at half filling reads $\sum_\sigma c^{\dagger}_{i\sigma}c_{i\sigma} = 1$.

The kinetic t-term built out of the physical electron operators given by equations (10) possesses the global Z_2 symmetry rather than the $SU(2)$ one.

Accordingly, the underlying onsite Hilbert space rearranges itself in the following way. The operators $\tilde{c}_{i\downarrow}$, $\tilde{c}^{\dagger}_{i\downarrow}$ act on the Hilbert space $\mathcal{H}_{\downarrow} = \{|\Downarrow, 0\rangle, |\Downarrow, \uparrow\rangle\}$. These operators do not mix any other states. Operator $\tilde{c}_{i\downarrow}$ destroys the spin-down electron and creates a vacancy. This vacancy is described by the state $|\Downarrow, \uparrow\rangle$. A similar consideration holds for the $\tilde{c}_{i\uparrow}$ operators. Now, however, the vacancy is described by the state $|\Uparrow, \downarrow\rangle$. These two vacancy states are related by the Z_2 transformation. The operator $(Q^z_i)^2 = \frac{1}{4}(1 - \tilde{n}^d_i)$ produces zero upon acting on both. The physical Hilbert state is therefore a direct sum $\mathcal{H}_{\rm ph} = \mathcal{H}_{\uparrow} \oplus \mathcal{H}_{\downarrow}$. Under the Z_2 transformation ($\uparrow \leftrightarrow \downarrow$, $S^z_i \rightarrow -S^z_i$) we get $\mathcal{H}_{\uparrow} \leftrightarrow \mathcal{H}_{\downarrow}$, which results in $\mathcal{H}_{\rm ph} \rightarrow \mathcal{H}_{\rm ph}$.[5]

As a result, one arrives at the representation (9) in which, however, the electron projection operators are given by equations (10). All the parts of this Hamiltonian possess the global discrete Z_2 symmetry whereas the global continuous $SU(2)$ symmetry is completely lost. Close to half filling this Hamiltonian reduces to the form

$$H^{\rm Ising}_{t-J} \equiv H_{t-J|_{Z_2}} = \sum_{ij\sigma} t_{ij}\tilde{d}^{\dagger}_{i\sigma}\tilde{d}_{j\sigma} + J\sum_{\langle ij\rangle}[(S^z_iS^z_j - \tfrac{1}{4}) + S^z_iM^z_j + S^z_jM^z_i], \tag{11}$$

which should be accompanied by the constraint

$$2S^z_iM^z_i + \tfrac{1}{2}\tilde{n}^d_i = 0. \tag{12}$$

In order to emphasize the difference between the t–J_z and the present model we dub the latter the Ising t–J or for short the t–$J|_{Z_2}$ model.

The factor of 2 which is presented in the hopping term of the isotropic t–J Hamiltonian (6) drops out from the hopping term in the Ising t–J Hamiltonian. This occurs because of the fact that the equations

$$\tilde{c}^{\dagger}_{i\uparrow} = \sqrt{2}\mathcal{P}^{\rm ph}_i\tilde{d}_{i\downarrow}\mathcal{P}^{\rm ph}_i,$$

$$\mathcal{P}^{\rm ph}_i = 1 - (\boldsymbol{S}_i\boldsymbol{M}_i + \tfrac{3}{4}\tilde{n}^d_i)$$

which are valid for both the t–J and t–J_z models, are in the t–$J|_{Z_2}$ model replaced by the following ones:

$$\tilde{c}^{\dagger}_{i\uparrow} = \mathcal{P}^{\rm ph}_i\tilde{d}_{i\downarrow}\mathcal{P}^{\rm ph}_i,$$

$$\mathcal{P}^{\rm ph}_i = 1 - (2S^z_iM^z_i + \tfrac{1}{2}\tilde{n}^d_i).$$

In practical calculations, the NDO constraint (12) can be taken into account with the help of a Lagrange multiplier. In order to do this we introduce an additional term to the Hamiltonian,

$$\lambda\sum_i(2S^z_iM^z_i + \tfrac{1}{2}n^d_i) = \lambda\sum_i[(\tfrac{1}{2} + S^z_i)d^{\dagger}_{i\uparrow}d_{i\uparrow} + (\tfrac{1}{2} - S^z_i)d^{\dagger}_{i\downarrow}d_{i\downarrow}]. \tag{13}$$

[5] In the isotropic t–J model these two 2D spaces merge into a 3D $SU(2)$ invariant physical space, where the vacancy is just an antisymmetric linear combination given by the $SU(2)$ spin singlet (5). The symmetric combination splits off, since it represents an unphysical spin-triplet state.

Notice that the operator $(\frac{1}{2} + S^z_i)d^{\dagger}_{i\uparrow}d_{i\uparrow} + (\frac{1}{2} - S^z_i)d^{\dagger}_{i\downarrow}d_{i\downarrow}$ produces eigenvalues 0 and 1, when acting on the onsite physical and unphysical states, respectively. Because of this, the global Lagrange multiplier $\lambda \rightarrow \infty$ enforces the NDO constraint locally. The double dopon occupancy of an arbitrary site results in an appearance of an unphysical state and hence enhances the total energy by λ. Therefore, in the large-λ limit all unphysical states are automatically eliminated and we can in this limit safely remove the tilde sign from the d operators. In the following section we show that this constraint is of crucial importance for the description of the AF order at finite doping.

2.3. Monte Carlo calculations

The total Hamiltonian takes the form

$$H^{\lambda}_{t-J|_{Z_2}} = H_{\uparrow} + H_{\downarrow} + J\sum_{\langle ij\rangle} S^z_iS^z_j + \text{const}, \tag{14}$$

with

$$H_{\uparrow} = \sum_{ij} t_{ij}d^{\dagger}_{i\uparrow}d_{j\uparrow} + \sum_i d^{\dagger}_{i\uparrow}d_{i\uparrow}\left[\lambda\left(\frac{1}{2} + S^z_i\right) + \frac{J}{2}\sum_{\langle j\rangle_i} S^z_j\right], \tag{15}$$

$$H_{\downarrow} = \sum_{ij} t_{ij}d^{\dagger}_{i\downarrow}d_{j\downarrow} + \sum_i d^{\dagger}_{i\downarrow}d_{i\downarrow}\left[\lambda\left(\frac{1}{2} - S^z_i\right) - \frac{J}{2}\sum_{\langle j\rangle_i} S^z_j\right], \tag{16}$$

where $\langle j\rangle_i$ denotes neighbouring sites of a given site i. We have neglected the hole–hole interaction in $H^{\lambda}_{t-J|_{Z_2}}$, which is perfectly justified in the low doping regime. In order to verify this approximation we have carried out additional calculations with the hole–hole interaction being taken into account in the mean-field approximation. The difference is negligible and therefore we do not present them here. Note that the interaction strength in $H^{\lambda}_{t-J|_{Z_2}}$ is exactly the same as in the standard formulation of the t–J model. Absence of any renormalization of the model parameters originates from the fact that the projection procedure is explicitly built into equation (14), provided $\lambda \rightarrow \infty$. Despite its complexity, with the Monte Carlo (MC) method, one can investigate the Hamiltonian (14) for very large systems without any approximation. Since $[S^z_i, H^{\lambda}_{t-J|_{Z_2}}] = 0$ the spin degrees of freedom can be analysed within the classical Metropolis algorithm. However, since the effective Hamiltonian (14) includes both fermionic as well as classical degrees of freedom, this algorithm needs to be modified. The procedure is as follows:

(i) an initial configuration of $\{S^z_i\}$ is generated;
(ii) the Hamiltonians (15), (16) are diagonalized and the free energy $\mathcal{F}$ of the fermionic subsystem in the canonical ensemble is determined;
(iii) two sites with opposite spins S^z are randomly chosen; then, both the spins are flipped;
(iv) step (ii) is repeated, determining a new value of the free energy $\mathcal{F}'$;
(v) if $\mathcal{F}' < \mathcal{F}$ or $\exp[(\mathcal{F} - \mathcal{F}')/kT] > x$, where x is a random number from the interval [0; 1), the new $\{S^z_i\}$ configuration is accepted, added to the ensemble and the procedure goes to step (iii), otherwise it goes directly to step (iii).

This is the Metropolis algorithm, but with the internal energy in statistical weights replaced by the free energy of the fermionic subsystem. A detailed description of this approach can be found in [27]. Concurrently with the MC simulation an iterate procedure calculating the distribution of holes is carried out in a self-consistent way.

Most of the numerical results have been obtained for a 20×20 system with periodic boundary conditions. However, in order to check the influence of finite-size effects we have carried out calculations on clusters of up to 1600 lattice sites and with averaging over the boundary conditions [28]. This problem is discussed at the end of the next section.

In order to eliminate the unphysical states in the Monte Carlo simulations, we have taken $\lambda = 100t$. Therefore, the Lagrange multiplier is by far the largest energy scale in the system, which guaranties the single occupancy of each lattice site. The simulations have been carried out in the canonical ensemble, which allows for accurate control of the doping level. We assume an absence of the ferromagnetic order. Namely, we take $\sum_i S_i^z = \sum_i M_i^z = 0$, what is reflected in the third point of the MC procedure.

The aim of the simulations is to determine how the antiferromagnetic order and the spectral properties are affected by doping. We start our discussion with the doping dependence of the spin–spin correlation function for the projected physical electron operators

$$g(r) = \frac{4}{N^2}\sum_i\sum_j \langle (S_i^z + M_i^z)(S_j^z + M_j^z)\rangle \times \exp[\mathrm{i}\boldsymbol{K}\cdot(\boldsymbol{R}_i - \boldsymbol{R}_j)]\bar{\delta}(r - |\boldsymbol{R}_i - \boldsymbol{R}_j|), \tag{17}$$

where $\boldsymbol{K} = (\pi, \pi)$ and

$$\bar{\delta}(x) = \begin{cases} 1 & \text{if } |x| \leqslant 0.5a, \\ 0 & \text{otherwise,} \end{cases}$$

with a being the lattice constant. $\langle\cdots\rangle$ in equation (17) means an average over the spin configurations generated in the MC run. $g(r)$ allows one to distinguish between the long-range order (LRO), when it remains finite for arbitrary r, quasi-long-range order (QLRO), when $g(r)$ decays algebraically, and short-range order (SRO), when $g(r)$ decays exponentially. Calculations of the spin–spin correlation function will be accompanied by results obtained for a static spin-structure factor, defined as

$$S(\boldsymbol{q}) = \frac{1}{N^2}\sum_{ij} \mathrm{e}^{\mathrm{i}\boldsymbol{q}(\boldsymbol{R}_i - \boldsymbol{R}_j)}\langle (S_i^z + M_i^z)(S_j^z + M_j^z)\rangle. \tag{18}$$

The third quantity that we use in the following discussion is the hole spectral function given by

$$A(\boldsymbol{k}, \omega) = -\frac{1}{\pi}\mathrm{Im}\, G(\boldsymbol{k}, \omega + \mathrm{i}0^+), \tag{19}$$

where

$$G(\boldsymbol{k}, z) = \sum_i\sum_j \exp\{\mathrm{i}\boldsymbol{k}(\boldsymbol{R}_i - \boldsymbol{R}_j)\} \times \langle \mathcal{G}_\sigma(\boldsymbol{R}_i, \boldsymbol{R}_j, z)[\tfrac{1}{2} - s(\sigma)S_i^z][\tfrac{1}{2} - s(\sigma)S_j^z]\rangle, \tag{20}$$

with $s(\uparrow) = 1$ and $s(\downarrow) = -1$. Here, similarly to equation (17), $\langle\cdots\rangle$ indicates averaging over spin configurations and

$$\mathcal{G}_\sigma(\boldsymbol{R}_i, \boldsymbol{R}_j, z) = \{[z - H_\sigma]^{-1}\}_{ij} \tag{21}$$

is the real-space Green function for a given spin configuration $\{S_i^z\}$. The presence of factors $\frac{1}{2} - s(\sigma)S_i^z$ in equation (20) follows from equation (10). Note that the spin–spin correlation function, the spin-structure factor and the spectral function are defined for physical electron operators, $\tilde{c}_i$.

3. Numerical results

3.1. Homogeneous systems

As discussed in the preceding sections the derived representation differs from the standard t–J_z Hamiltonian in that the $SU(2)$ symmetry is broken also for $J = 0$. In order to visualize the physical consequences of this difference we start with calculations for the one-hole case. In this regime large clusters have been analysed numerically both for the t–J_z and t–J models.

In the main panel of figure 1 we show the one-hole energy calculated at $T = 0$ for an 8×8 cluster without the $\frac{1}{4}\tilde{n}_i\tilde{n}_j$ term. Here, we compare our data with exact results obtained for a 50-site t–J_z cluster [29] as well as with recent exact results for a bulk t–J system [11]. In the inset of figure 1 we compare exact results obtained for 4×4 t–$J|_{Z_2}$ and t–J_z clusters [30] for a wider range of the J/t ratio. In two limiting cases $J/t \to 0$ and $J/t \to \infty$ the one-hole energy obtained in our approach is the same as in the t–J_z model. It can be explained in the following way. For $J = 0$, the ferromagnetic Nagaoka state becomes a ground state in both the approaches. In this case the propagation of a hole is not perturbed by the magnetic order and the one-hole energy equals $-4t$. The main difference between t–J_z and t–$J|_{Z_2}$ approaches consists in the symmetry of the hopping term. Therefore, they merge in the case $J/t \gg 1$, when the system properties are determined predominantly by the same spin–spin interaction. In the regime of intermediate J the differences are most pronounced. The one-hole energy obtained for the t–J model in this regime is in between the results obtained for t–J_z and t–$J|_{Z_2}$ approaches. Here, the differences between t–J and t–J_z models are comparable to those between t–J and t–$J|_{Z_2}$ ones.

Next, we investigate how the doping affects the antiferromagnetic order. The previous studies of the t–J model clearly indicate that the long-range hopping amplitudes significantly modify the bandwidth and the dispersion of the quasiparticles [31]. Recent Green's function Monte Carlo calculations demonstrate that the next nearest neighbour hopping reduces the critical doping at which the AF LRO disappears [14]. The importance of these results follows from the fact that in the t–J model with only the nearest neighbour hopping, antiferromagnetic correlations persist up to hole concentrations much larger than the ones observed in HTSC materials. One may expect that in the absence of the transverse spin–spin interaction the robustness of LRO should be even

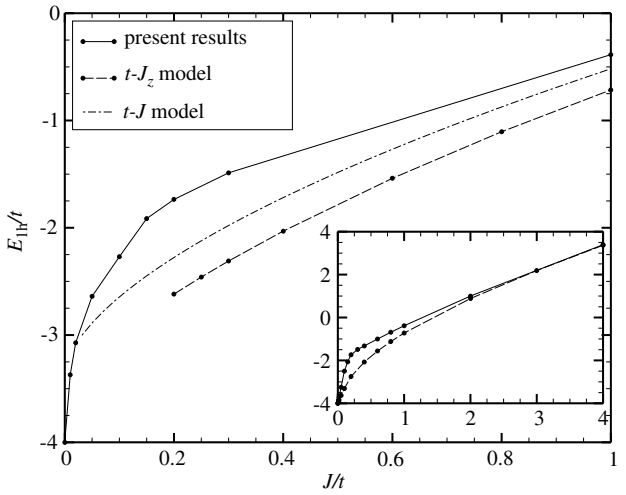

Figure 1. One-hole energy as a function of J/t for a 8×8 cluster at $T = 0$. The data labelled as t–J_z and t–J have been taken from [29] and [11], respectively. In the latter case, it is the energy of a hole with momentum $(\pi/2, \pi/2)$. The inset shows results obtained for 4×4 t–$J|_{Z_2}$ and t–J_z systems. Here, the dashed line shows results presented in [30] for the t–J_z model. Since for $J \to 0$ the ferromagnetic order sets in, the constraint $\sum_i S_i^z = 0$ is now relaxed.

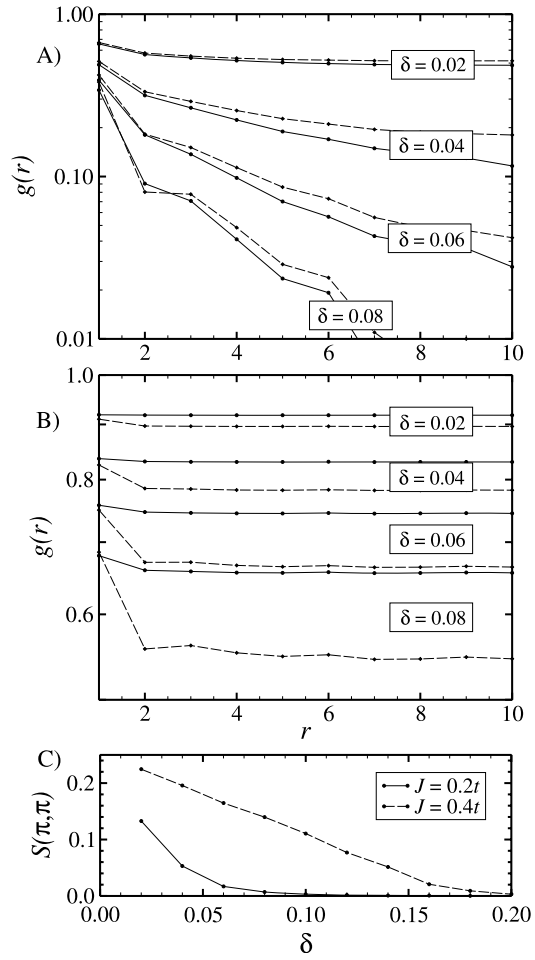

Figure 2. Panels (A) and (B) show $g(r)$ calculated for $kT = 0.1t$. $J = 0.2t$ (A) and $J = 0.4t$ (B). The curves from the top to the bottom have been obtained for $\delta = 0.02, 0.04, 0.06, 0.08$. Solid (dashed) lines show results obtained for $t' = t'' = 0$ ($t' = -0.27t$ and $t'' = 0.2t$). Panel (C) shows the doping dependence of the static spin-structure factor $S(\pi, \pi)$ at $kT = 0.1t$ for $t' = -0.27t$ and $t'' = 0.2t$.

more pronounced. Moreover, the previous analysis of the one- and two-hole spectra in the t–J_z model [20] has shown that for $t/J < 5$ half of the one-hole band width does not exceed $0.08t$. Therefore, the intra-sublattice hopping should be a source of an important contribution to the kinetic energy even for small values of the second- t' and third- t'' nearest-neighbour hopping integrals. The significance of the long-range hopping for the AF order is demonstrated in figure 2, where we compare the spin–spin correlation functions calculated with and without t' and t''. In all the figures showing $g(r)$ we use a logarithmic scale for the vertical axis. Therefore, for LRO, QLRO and SRO, $g(r)$ should be represented asymptotically by a constant function, a logarithmic function and a straight line, respectively. In the following, δ denotes the average concentration of holes.

One can see that the influence of the long-range hopping depends, even qualitatively, on the value of the exchange coupling J. For a small value of J, the AF order is *enhanced* when hoppings to second- and third-nearest neighbours are allowed (for $J = 0.2t$ see panel (A) in figure 2). On the other hand, for bigger values of J, these hoppings *reduce* the AF order (for $J = 0.4t$ see panel (B) in figure 2). Such a behaviour could be explained as follows. In the presence of only nearest-neighbour hopping there is a strong competition between the energy of spin–spin interaction and the hole kinetic energy. This results from the fact that in this case only inter-sublattice hopping is allowed. From equation (13) one can then infer that it is possible only in regions where the AF order is absent. Then, nonzero t' and t'' allow for intra-sublattice hopping, thereby leading to gaining of the kinetic energy without destroying the AF order. This mechanism is effective for $J \leqslant 0.25t$. On the other hand, for $t' = t'' = 0$ and large J, holes are almost localized and, therefore, only weakly frustrate the AF state. The intra-sublattice hopping allows for the propagation of holes, which effectively reduces the AF LRO.

The doping-induced destruction of the AF LRO can directly be seen in figure 2(C), where we present the spin-structure factor obtained for $t' = -0.27t$ and $t'' = 0.2t$. This quantity is important in that it is directly accessible in, e.g., neutron scattering experiments. The maximal doping for which the AF state still exists strongly depends on the magnitude of the exchange interaction. This result contrasts with the recently reported Green's function Monte Carlo study of the t–J model [14], where the AF LRO vanishes at $\delta = 0.1$ and $\delta = 0.13$ for $J = 0.2t$ and $J = 0.4t$, respectively. In our approach the experimental data for the critical doping in HTSC can be reproduced provided $J < 0.2t$.

In order to illustrate the interplay between the AF order and the mobility of holes we have calculated the hole spectral functions $A(\boldsymbol{k}, \omega)$ (see figures 3, 4). For $t' = t'' = 0$ and small δ one can see almost localized particles with very small dispersion. A similar situation occurs in the t–J_z model, but it is not the case for the t–J one, where the spin-flip term

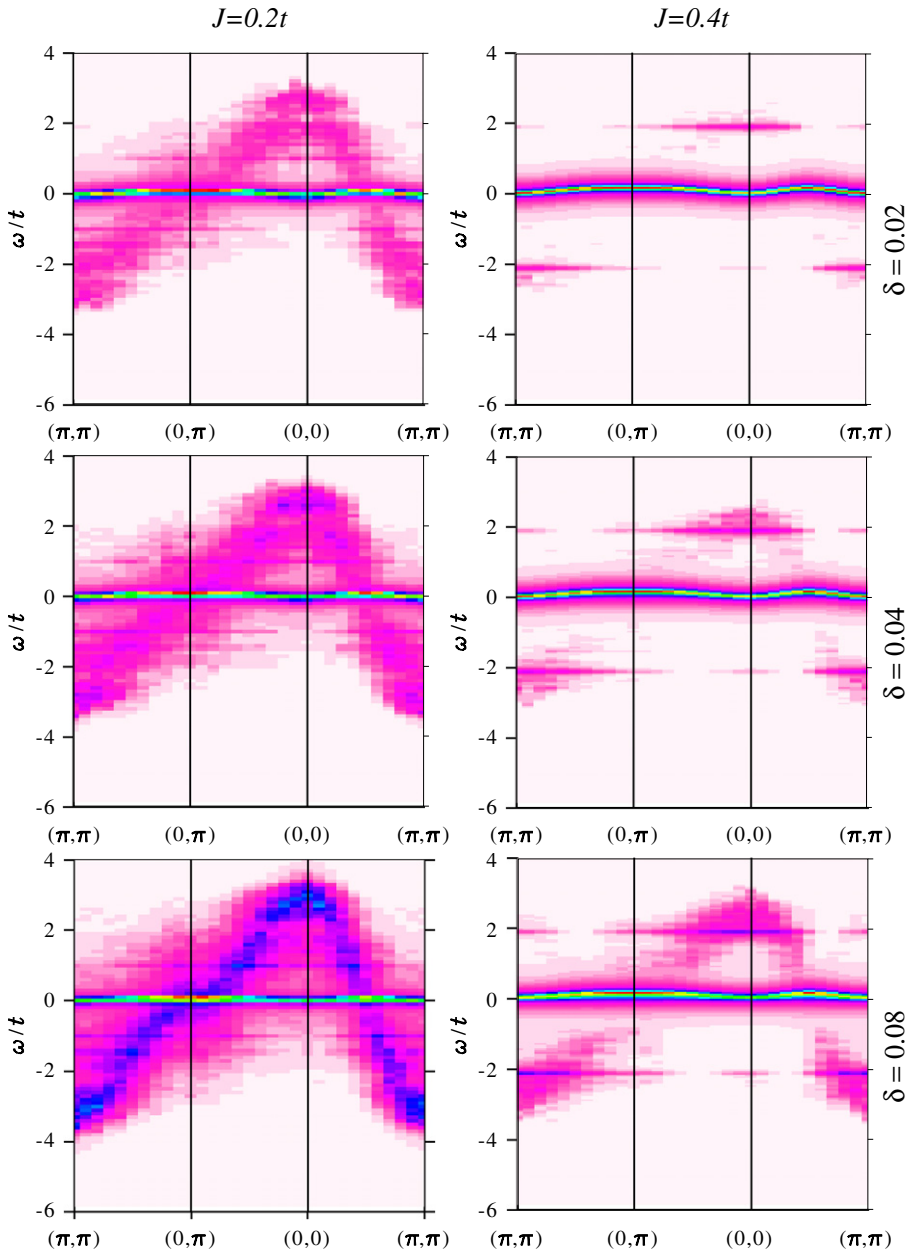

Figure 3. Spectral functions $A(\boldsymbol{k}, \omega)$ calculated for $kT = 0.1t$ along the main symmetry lines of the Brillouin zone with $t' = t'' = 0$.

can undo the defects generated by a moving hole and hence it allows for its much higher mobility. In the present approach holes become mobile when doping increases, i.e. when the AF background disappears. The onset of mobile holes is accomplished through a gradual transfer of the spectral weight from the vicinity of the almost localized level. Close to half filling the most significant transfer takes place in states with $\boldsymbol{k} = (0, 0)$ and $\boldsymbol{k} = (\pi, \pi)$. However, even for relatively large doping the spectral functions remain broad for all the momenta.

For nonzero t' and t'' there are mobile holes even for small doping, but the spectral functions still remain very broad. Also in this case, doping is responsible for significant modification of the dispersion relation of holes. In figure 4 we compare $A(\boldsymbol{k}, \omega)$ calculated for $\delta = 0.02, \ldots, 0.14$ with $t' = -0.27t$ and $t'' = 0.2t$. Along with the destruction of the AF LRO, there is an increasing contribution of nearest neighbour hopping to the hole kinetic energy. For $\delta = 0.02$ the peaks in spectral functions can be fitted by the dispersion relation with $t = 0$, whereas for $\delta = 0.14$ the AF correlations hardly influence the nearest neighbour hopping. Note that such a substantial modification of the dispersion relation may change the topology of the Fermi surface. Doping affects not only the effective dispersion relation, but also frustrates the AF background. The latter effect is responsible for strong broadening of the spectral functions that is visible in figure 4. Comparison of figure 2 with figures 3 and 4 demonstrates that the mobility of holes and destruction of the AF LRO are mutually connected with each other in the sense that mobility affects AF LRO and, vice versa, AF order affects the mobility of holes.

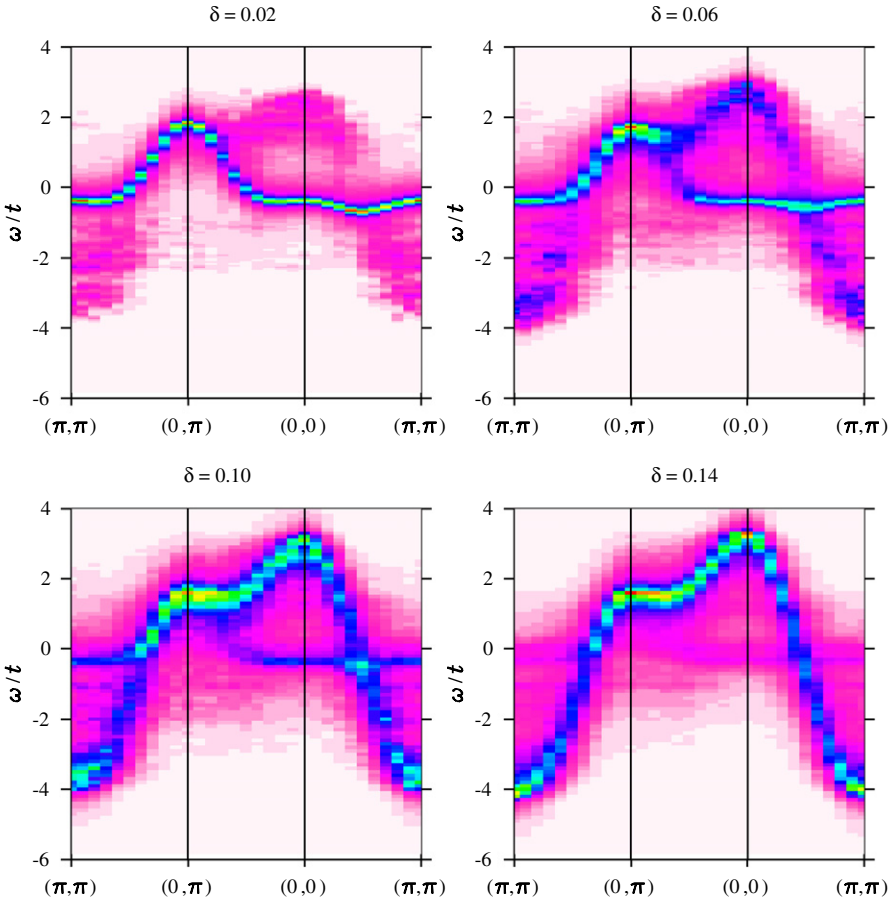

Figure 4. Spectral functions $A(\boldsymbol{k}, \omega)$ calculated along the main symmetry lines of the Brillouin zone for $J = 0.2t$, $kT = 0.1t$ and various dopings. $t' = -0.27t$ and $t'' = 0.2t$ have been assumed.

We now turn our attention to the temperature dependence of the spin–spin correlation function and the spectral properties of holes. It is known that the Néel temperature drops rapidly when the parent compounds of the high-temperature superconductors are doped with holes. Similar behaviour can be inferred from figure 5, where the temperature dependence of $g(r)$ is presented for different doping levels. One can note that doping strongly reduces the LRO, whereas its influence on the SRO is much weaker. In particular, the nearest neighbour correlation functions $g(1)$ calculated for $\delta = 0.02$ and $\delta = 0.06$ are qualitatively and quantitatively close to each other. These results suggest that the AF SRO should be observed in a wide range of temperatures and dopings, much beyond the boundaries of the AF phase. This remains in agreement with recent experiments on high-temperature superconductors suggesting that with doping the long-range Néel order gives way to short-range order with a progressively shorter correlation length. As a result, at optimal doping the static spin correlation length is no more than two or three lattice spacings [32].

The correlation function discussed above and the spin-structure factor describe the background composed of the localized spins, which, as mentioned in the preceding paragraphs, is to some degree affected by the motion of doped holes. Therefore, the reduction of the antiferromagnetic correlations has to be observed also in the dynamics of the carriers. It is shown in figure 6, where we demonstrate the temperature dependence of the spectral functions. When the temperature increases, the number of spin defects in the Néel state increases as well, and this enables the nearest neighbour hopping, thereby allowing holes to lower their kinetic energy. This mechanism leads to trapping of holes in the regions of broken antiferromagnetic bonds and forming ferromagnetic spin polarons, where the hole hopping does not frustrate the spin background. The contribution of the nearest neighbour hopping becomes visible in the spectral functions, where the increase of the temperature causes a significant broadening of the spectral lines. Similarly to the spectral functions obtained for a single hole in the t–t'–t''–J model [33], the width of the peaks in the $A(\boldsymbol{k}, \omega)$ is too small when compared to the results of the angle–resolved spectroscopy (ARPES) measurements [34] on $Sr_2CuO_2Cl_2$. It has recently been argued that strong electron–phonon interaction [35, 36] may explain the very broad peaks observed in the insulating copper oxides [37, 38].

In the present approach, holes interact with spins through the intersite interaction of strength J as well as through the onsite constraint with the Lagrange multiplier λ, and both of these interactions can be responsible for the destruction of the AF LRO. In order to determine the underlying mechanism we

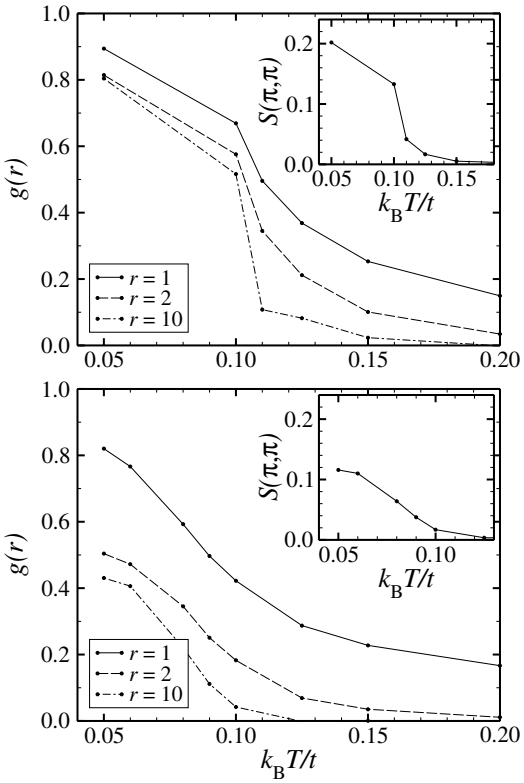

Figure 5. $g(r)$ as a function of temperature for $J = 0.2t$ and $\delta = 0.02$ (upper panel) and $\delta = 0.06$ (lower panel). The lines from the top to the bottom show $g(1)$, $g(2)$ and $g(10)$. $t' = -0.27t$ and $t'' = 0.2t$ have been assumed.

have carried out simulations taking into account one of these interactions at a time. The results shown in the upper panel of figure 7 clearly demonstrate that the constraint plays the dominating role in the destruction of the AF state. When both these interactions are taken into account the LRO is completely destroyed and only AF SRO can be observed for $\delta = 0.08$. However, if we ignore the constraint, LRO is restored. The results obtained without the intersite spin–hole interaction ($S_i^z M_j^z$ terms) are almost indistinguishable from the ones obtained with both the interactions. Note that for $\lambda = 0$ the NDO constraint is completely neglected. This illustrates the importance of the constraint for a realistic description of the AF order at finite doping. Additionally, in order to determine the value of the Lagrange multiplier for which the results converge and the NDO constraint is fulfilled, we have calculated $g(r)$ for a wide range of λ. The results are presented in the lower panel of figure 7. One can see that the assumed value $\lambda = 100t$ is large enough to enforce the constraint. After explaining the role of the farther neighbour hopping we restrict the following analysis to the case of $t' = -0.27t$ and $t'' = 0.2t$.

3.2. Inhomogeneous systems

Since our method works for systems with broken translational invariance, it is tempting to apply it as well to inhomogeneous systems. It has recently been shown with the help of scanning tunnelling spectroscopy that nanoscale electronic inhomogeneity is an inherent feature of many groups of high-temperature superconductors. By a direct probing of the local density of states, these methods reveal strong spatial modulation of the energy gap in the superconducting Bi-based compounds [39]. Very recently, STM experiments have shown a strong correlation between position of the dopant atoms and all manifestations of the nanoscale electronic disorder [40, 41]. Thus, these experiments proved essentially that the impurities were the source of the inhomogeneity. On the other hand, they revealed a very important feature: there is a *positive* correlation between the magnitude of a gap and the position of an out-of-plane oxygen atom [40]. These are the atoms which have been doped into the insulating parent compound in order to introduce holes to the CuO_2 planes. The gap–impurity correlation has been explained as a result of the inhomogeneity-enhanced exchange interaction in the t–J model [42]. Assuming that purely electronic models contain the essential physics of cuprates, the same interaction is responsible for both superconductivity and the AF order. Therefore, inhomogeneity may affect the AF state as well. Additionally, localization of holes by the electrostatic potential of out-of-plane oxygen atoms may also affect the AF order, since the hopping of holes frustrates the AF LRO. In the following, we investigate the role played by these mechanisms in the strongly underdoped regime. In order to investigate the latter one, we extend the Hamiltonian (14) by adding a term responsible for inhomogeneity-induced diagonal disorder

$$H^{\lambda}_{t-J|_{z_2}} \to H^{\lambda}_{t-J|_{z_2}} + \sum_{i\sigma} \varepsilon_i d^{\dagger}_{i\sigma} d_{i\sigma}, \tag{22}$$

where

$$\varepsilon_i = \begin{cases} V, & \text{if there is an out-of-plane oxygen atom} \\ & \quad \text{above site } i, \\ 0, & \text{otherwise.} \end{cases}$$

Since in HTSCs each doped oxygen atom introduces one hole in the CuO_2 plane, we have carried out calculations for the number of impurities equal to the number of holes. Technically, for each Monte Carlo simulation we generate a random configuration of the out-of-plane oxygen atoms and keep it frozen during the whole run. In this way both holes and localized spins feel a quenched disorder.

In the upper panel of figure 8 we show a comparison of the correlation function $g(r)$ calculated in the presence of the diagonal disorder and without it. From this figure one sees that the influence of the diagonal disorder is almost negligible, at least for small-to-moderate values of the potential V. For larger values of V, the presence of negatively charged out-of-plane oxygen atoms reduces the hole mobility, resulting in a visible enhancement of the spin–spin correlation function. It is worthwhile to emphasize that the NDO constraint becomes very important in the presence of the diagonal disorder despite the low concentration of holes. In a homogeneous system with $\delta \ll 1$ this constraint is less important as the probability of double-hole occupancy is proportional to δ^2. Since the negatively charged out-of-plane oxygen atoms locally enhance

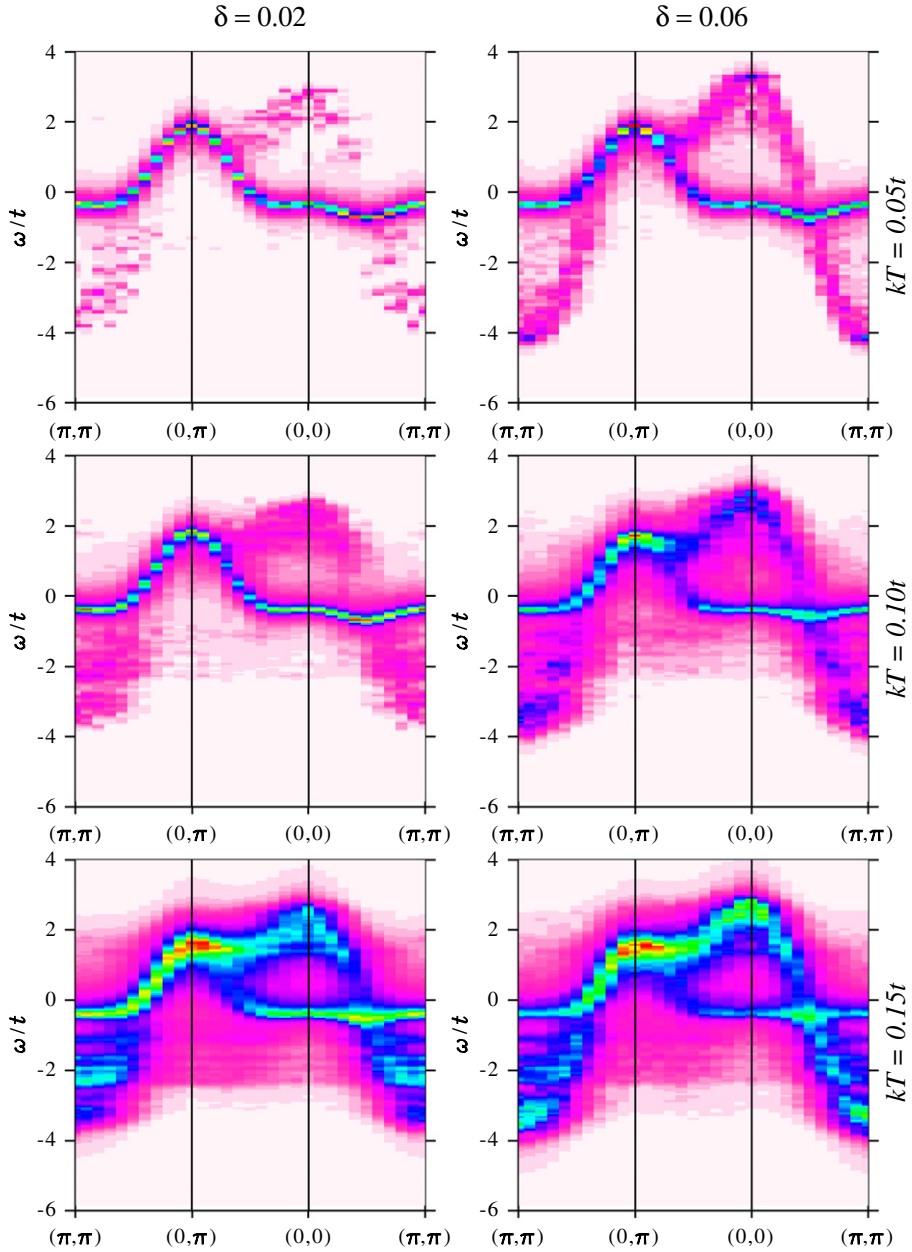

Figure 6. Spectral functions $A(\boldsymbol{k}, \omega)$ calculated along the main symmetry lines of the Brillouin zone for $J = 0.2t$. $t' = -0.27t$ and $t'' = 0.2t$ have been assumed.

the hole concentration, neglecting the NDO may significantly modify the results [42].

Now we turn to the influence of the inhomogeneity-induced enhancement of the exchange interaction. Following the results of [42] we assume J to a be site-dependent quantity:

$$J_{ij} = J\ \left(1 + \eta_{ij}\right), \tag{23}$$

where

$$\eta_{ij} = \begin{cases} \eta > 0, & \text{if there is an out-of-plane oxygen atom} \\ & \text{above site } i \text{ or } j, \\ 0, & \text{otherwise.} \end{cases}$$

In contrast with the superconducting gap [42], the AF order is hardly modified by this mechanism. This can be clearly inferred from the lower panel in figure 8. The regime for a magnetic ordering predicted by many calculations in the t–J model extends to much larger dopings than observed in cuprates, and this discrepancy is sometimes attributed to the inhomogeneities, which are neglected in many theoretical approaches (see the discussion in [14]). Although inhomogeneities are expected to play an important role in high-temperature superconductors [25], our results indicate that their influence in the AF ordering is rather limited. In particular, we expect that the inhomogeneities introduced by the out-of-plane oxygen atoms cannot explain the above discrepancy.

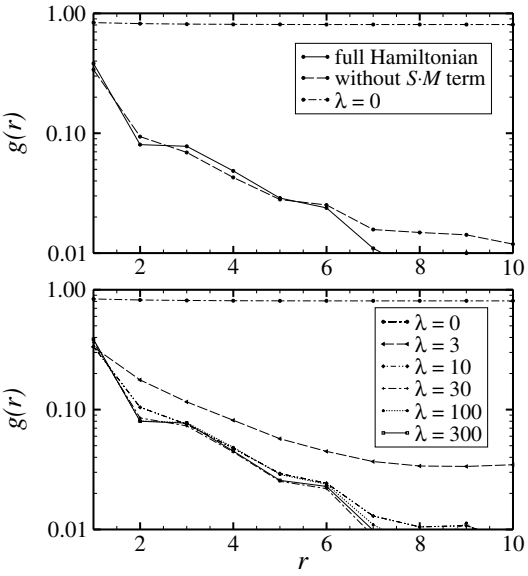

Figure 7. $g(r)$ for $J = 0.2t, kT = 0.1t, \delta = 0.08, t' = -0.27t$ and $t'' = 0.2t$. In the upper panel the topmost curve has been calculated with $\lambda = 0$. The other curves show results obtained for $\lambda = 100t$ with and without the spin–hole exchange interaction. The lower panel shows $g(r)$ for different values of λ. Note that the results for $\lambda = 100t$ and $300t$ are almost indistinguishable.

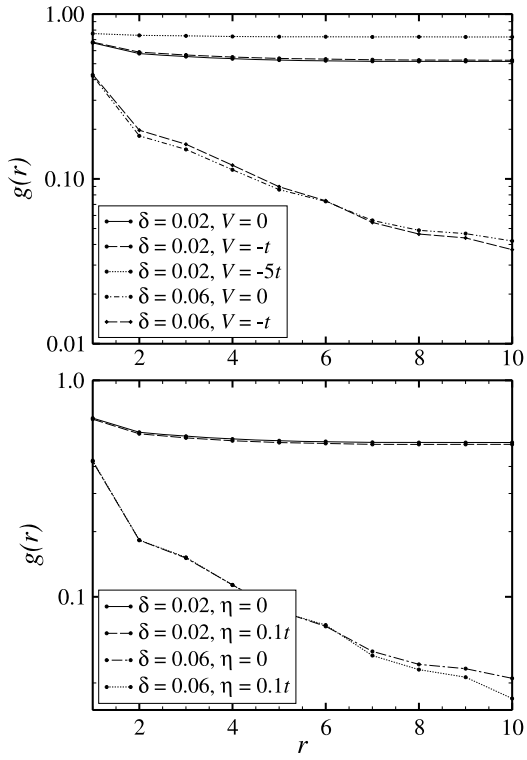

Figure 8. $g(r)$ for $J = 0.2t$ in the presence of the out-of-plane oxygen atoms. The upper panel demonstrates the influence of the diagonal disorder, whereas the lower panel shows effects coming from the site-dependent exchange interaction. The model parameters (δ, V, η) are given in the legend.

3.3. Finite-size effects

Since our analysis has been carried out on finite clusters, it is necessary to check to what extent the results are affected by the finite-size effects. One of the measures of the significance of the finite-size effects is a sensitivity to the boundary conditions. Therefore, we have calculated the correlation functions and the spectral functions for systems with different boundary conditions and compared them to those which have been obtained with periodic boundary conditions. Here, we have used a method known as averaging over boundary conditions (ABC) [28]. Each time a particular hole jumps out of the cluster, it is mapped back into the cluster with wavefunction with a different phase. Then the results are averaged over these phases; thereby, the reciprocal space is probed at a much greater number of points than in the case of periodic boundary conditions. In our simulations we have used a slightly modified version, where the phases were chosen randomly in each Monte Carlo step. The averaging over the boundary conditions has been carried out concurrently with averaging over the ensemble generated in Monte Carlo run [43]. This way it does not require an additional computational effort.

Another more direct way to check the influence of the finite-size effects is to compare results obtained on clusters of different sizes. In order to do so, we have repeated some calculations on 40×40 cluster. Figure 9 shows a comparison of spectral functions obtained for 20×20 and 40×40 clusters with periodic boundary conditions as well as for a 20×20 cluster with ABC. Since the false-colour plots of these spectral functions are very similar to each other, we present their energy dependence for a few selected points of the Brillouin zone. One can see from this figure that the coherent part of the spectral functions is almost exactly the same in these three cases. The low-intensity parts also look very similar, though some differences can be seen. Another quantity we have used to analyse the finite-size effects is the correlation function $g(r)$. Figure 10 shows $g(r)$ determined for the same three systems for which the spectral functions are presented in figure 9. Despite minor quantitative differences the overall character of all three correlation functions is the same. Though we have not carried out a systematic finite-size scaling, the similarity of both the spectral functions and the correlation functions constitutes a significant indication that our results are also valid in the thermodynamic limit.

4. Summary

We have developed a doped-carrier representation of the Ising t–J model. In this formulation, the system is described in terms of fermions interacting with static localized spins. Although it is a slave-particle approach, in contrast with many similar approaches, the local NDO constraint is taken into account exactly. The proposed Hamiltonian has the global Z_2 symmetry at any values of the parameters, J and t. This model is of interest in itself since it represents a simple though nontrivial electron system which captures the physics of strong electron correlations. The issue of how these correlations affect the magnetic ordering of the lattice spins is thoroughly investigated in the present work. Besides, this model may

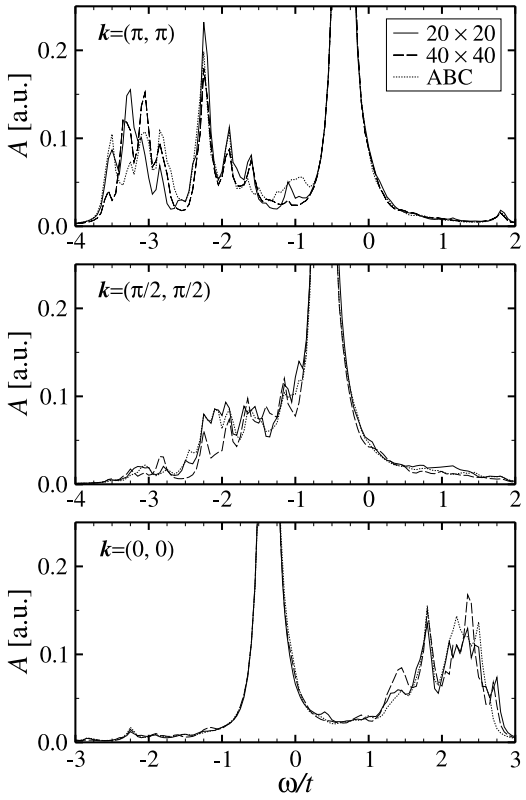

Figure 9. Spectral functions calculated for selected points of the Brillouin zone. These results have been obtained on 20×20 (solid line) and 40×40 (dashed line) clusters with periodic boundary conditions and on a 20×20 cluster with ABC (dotted line). Since the positions of the coherent peaks obtained with the help of these three approaches are almost indistinguishable, we have cut the vertical axis in such a way that the incoherent parts are more pronounced. These results have been obtained for $J = 0.2t$, $kT = 0.1t$, and $\delta = 0.02$.

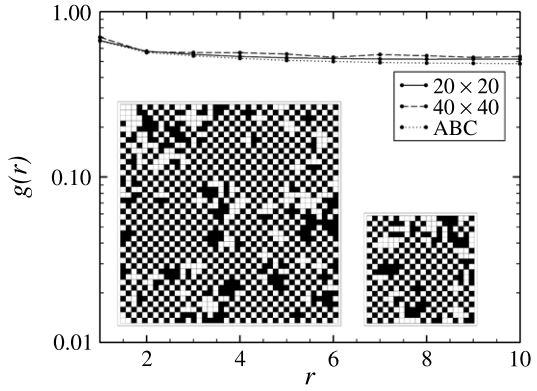

Figure 10. Correlation function $g(r)$ for the same systems as in figure 9. Also, the same parameters have been used. The insets show examples of snapshots of the spin configurations for 40×40 and 20×20 clusters (black (white) square corresponds to $S_i^z = \frac{1}{2}(S_i^z = -\frac{1}{2})$).

provide at least for some values of the model parameters a guess supported by unbiased numerical calculations regarding the actual low-energy behaviour of the quasiparticle excitations in a more realistic isotropic t–J model.

In particular, we have calculated the one-hole energy and compared our results with those obtained for t–J_z and t–J models. We have found that the one-hole energy is the same as in the t–J_z model in two limiting cases, $J \to 0$ and $J \to \infty$. For intermediate J the one-hole energy obtained for the t–J model is in between the results obtained for t–J_z and t–$J|_{Z_2}$ approaches and the differences between t–J and t–J_z models are comparable to those between t–J and t–$J|_{Z_2}$ ones.

The main advantage of the present approach consists in that it can be applied for very large systems and the computational effort increases much more slowly with the size of the system than, e.g., for exact diagonalization. Moreover, it works for arbitrary value of the coupling J and for arbitrary doping level. In particular, in the small-J regime the exact diagonalization and quantum Monte Carlo methods give rather poor results. This is because of the fact that in this regime the size of the defects generated by moving holes is comparable to or larger than the size of cluster the calculations can be carried out on. Since the clusters in our approach are much larger, this problem is less significant. Additionally, our method does not require translational invariance of the system. This feature is especially important in the context of the recent experimental results, which clearly indicate the presence of inhomogeneities in cuprates. It could also be applicable to optical lattices, where the translational symmetry is broken by a trap.

Using the proposed approach we have found that the AF SRO persists for temperatures and dopings which are much beyond the boundaries of the AF LRO phase, which is in agreement with recent experiments on the high-temperature superconductors. We have also demonstrated that the AF LRO depends on the exchange interaction J. It concerns the transition temperature as well as the maximal doping at which the AF LRO vanishes. We explicitly demonstrate that the local no-double-occupancy constraint plays the dominant role in destroying the magnetic order at finite doping.

Finally, we have shown that the inhomogeneities induced by the out-of-plane oxygen atoms have a rather limited influence on the spin–spin correlation functions, at least in the underdoped regime. Although localization of holes by their electrostatic potential stabilizes the AF LRO, this mechanism becomes important only for a relatively strong diagonal disorder. Such a limited influence of inhomogeneities on the AF order is closely related to the NDO constraint. Note that exactly at half filling the diagonal disorder does not influence the system, provided the NDO is properly taken into account.

Acknowledgments

This work has been supported by the Bogolyubov–Infeld programme and by the Polish Ministry of Education and Science under grant No 1 P03B 071 30.

References

[1] Schmitt-Rink S, Varma C M and Ruckenstein A E 1988 *Phys. Rev. Lett.* **60** 2793
[2] Shraiman B I and Siggia E D 1988 *Phys. Rev. Lett.* **60** 740
[3] Trugman S A 1988 *Phys. Rev.* B **37** 1597

[4] Wróbel P and Eder R 1998 *Phys. Rev.* B **58** 15160
[5] Dagotto E, Joynt R, Moreo A, Bacci S and Gagliano E 1990 *Phys. Rev.* B **41** 9049
[6] Prelovsěk P, Sega I and Bonča J 1990 *Phys. Rev.* B **42** 10706
[7] Martinez G and Horsch P 1991 *Phys. Rev.* B **44** 317
[8] Poilblanc D, Ziman T, Schulz H J and Dagotto E 1993 *Phys. Rev.* B **47** 14267
[9] Leung P W and Gooding R J 1995 *Phys. Rev.* B **52** R15711
[10] Brunner M, Assaad F F and Muramatsu A 2000 *Phys. Rev.* B **62** 15480
[11] Bonča J, Maekawa S and Tohyama T 2007 *Phys. Rev.* B **76** 035121
[12] Lugas M, Spanu L, Becca F and Sorella S 2006 *Phys. Rev.* B **74** 165122
[13] Morinari T 2004 *J. Magn. Magn. Mater.* **281** 188
[14] Spanu L, Lugas M, Becca F and Sorella S 2008 *Phys. Rev.* B **77** 024510
[15] Dagotto E 1994 *Rev. Mod. Phys.* **66** 763
[16] Chernyshev A L, White S R and Castro Neto A H 2002 *Phys. Rev.* B **65** 214527
[17] Chernyshev A L, Castro Neto A H and White S R 2005 *Phys. Rev. Lett.* **94** 036407
[18] Riera J A 2001 *Phys. Rev.* B **64** 104520
[19] Martins G B, Gazza C and Dagotto E 2000 *Phys. Rev.* B **62** 13926
[20] Chernyshev A L and Leung P W 1999 *Phys. Rev.* B **60** 1592
[21] Elrick B M and Jacobs A E 1995 *Phys. Rev.* B **52** 10369
[22] Ribeiro T C and Wen X-G 2005 *Phys. Rev. Lett.* **95** 057001
Ribeiro T C and Wen X-G 2006 *Phys. Rev.* B **74** 155113
[23] Ferraz A, Kochetov E and Mierzejewski M 2006 *Phys. Rev.* B **73** 064516
[24] Pepino R T, Ferraz A and Kochetov E 2008 *Phys. Rev.* B **77** 035130
[25] Dagotto E 2005 *Science* **309** 257
[26] Chao K A, Spałek J and Oleś A M 1978 *Phys. Rev.* B **18** 3453
[27] Maśka M M and Czajka K 2006 *Phys. Rev.* B **74** 035109
[28] Poilblanc D 1991 *Phys. Rev.* B **44** 9562
Gros C 1992 *Z. Phys.* B **86** 359
Gros C 1996 *Phys. Rev.* B **53** 6865
Czajka K and Maśka M 2004 *Acta Phys. Pol.* A **106** 703
[29] Riera J and Dagotto E 1993 *Phys. Rev.* B **47** 15346
[30] Barnes T, Dagotto E, Moreo A and Swanson E S 1989 *Phys. Rev.* B **40** 10977
[31] Bała J, Oleś A M and Zaanen J 1995 *Phys. Rev.* B **52** 4597
Xiang T and Wheatley J M 1996 *Phys. Rev.* B **54** R12 653
Kyung B and Ferrell R A 1996 *Phys. Rev.* B **54** 10125
Lee T K and Shih C T 1997 *Phys. Rev.* B **55** 5983
Lee T K, Ho C-M and Nagaosa N 2003 *Phys. Rev. Lett.* **90** 067001
Danmascelli A, Shen Z-X and Hussain Z 2003 *Rev. Mod. Phys.* **75** 473
[32] Regnault L P, Bourges P and Burlet P 1998 *Neutron Scattering in Layered Copper-Oxide Superconductors* ed A Furrer (Amsterdam: Kluwer)
Kastner M A, Birgeneau R J, Shiran G and Endoh Y 1998 *Rev. Mod. Phys.* **70** 897
Aeppli G, Mason T E, Hayden S M, Mook H A and Kulda J 1997 *Science* **278** 1432
Curro N J, Imai T, Slichter C P and Dabrowski B 1997 *Phys. Rev.* B **56** 877
[33] van den Brink J and Sushkov O P 1998 *Phys. Rev.* B **57** 3518
[34] Wells B O, Shen Z-X, Matsuura A, King D M, Kastner M A, Greven M and Birgeneau R J 1995 *Phys. Rev. Lett.* **74** 964
Pothuizen J J M, Eder R, Hien N T, Matoba M, Menovsky A A and Sawatzky G A 1997 *Phys. Rev. Lett.* **78** 717
[35] Cataudella V, De Filippis G, Mishchenko A S and Nagaosa N 2007 *Phys. Rev. Lett.* **99** 226402
[36] Bonča J, Maekawa S, Tohyama T and Prelovšek P 2008 *Phys. Rev.* B **77** 054519
[37] Shen K M, Ronning F, Lu D H, Lee W S, Ingle N J C, Meevasana W, Baumberger F, Damascelli A, Armitage N P, Miller L L, Kohsaka Y, Azuma M, Takano M, Takagi H and Shen Z-X 2004 *Phys. Rev. Lett.* **93** 267002
[38] Shen K M, Ronning F, Meevasana W, Lu D H, Ingle N J C, Baumberger F, Lee W S, Miller L L, Kohsaka Y, Azuma M, Takano M, Takagi H and Shen Z-X 2007 *Phys. Rev.* B **75** 075115
[39] Pan S H, O'Neal J P, Badzey R L, Chamon C, Ding H, Engelbrecht J R, Wang Z, Eisaki H, Uchida S, Guptak A K, Ngk K-W, Hudson E W, Lang K M and Davis J C 2001 *Nature* **413** 282
[40] McElroy K, Lee J, Slezak J A, Lee D-H, Eisaki H, Uchida S and Davis J C 2005 *Science* **309** 1048
[41] Mashima H, Fukuo N, Matsumoto Y, Kinoda G, Kondo T, Ikuta H, Hitosugi T and Hasegawa T 2006 *Phys. Rev.* B **73** 060502(R)
[42] Maśka M M, Śledź Ż, Czajka K and Mierzejewski M 2007 *Phys. Rev. Lett.* **99** 147006
[43] Czajka K and Maśka M M 2007 *Phys. Status Solidi* b **244** 2427